



Sediments and bedforms of the Harle tidal inlet (Wadden Sea, Germany)

Francesco Mascioli, Valerio Piattelli, Francesco Cerrone, Jacopo Cinosi, Tina Kunde & Enrico Miccadei

To cite this article: Francesco Mascioli, Valerio Piattelli, Francesco Cerrone, Jacopo Cinosi, Tina Kunde & Enrico Miccadei (2022): Sediments and bedforms of the Harle tidal inlet (Wadden Sea, Germany), Journal of Maps, DOI: [10.1080/17445647.2022.2154175](https://doi.org/10.1080/17445647.2022.2154175)

To link to this article: <https://doi.org/10.1080/17445647.2022.2154175>



© 2022 The Author(s). Published by Informa UK Limited, trading as Taylor & Francis Group on behalf of Journal of Maps



[View supplementary material](#)



Published online: 31 Dec 2022.



[Submit your article to this journal](#)



Article views: 459



[View related articles](#)



[View Crossmark data](#)



Citing articles: 1 [View citing articles](#)



Sediments and bedforms of the Harle tidal inlet (Wadden Sea, Germany)

Francesco Mascioli ^a, Valerio Piattelli ^b, Francesco Cerrone ^b, Jacopo Cinosi ^b, Tina Kunde ^a and Enrico Miccadei ^b

^aNLWKN, Coastal Research Station, Lower Saxony Water Management, Coastal Defence and Nature Conservation Agency, Norden, Germany; ^bDepartment of Engineering and Geology, Laboratory of Tectonic Geomorphology and GIS, Università degli Studi 'G. d'Annunzio' Chieti-Pescara, Chieti Scalo, Italy

ABSTRACT

The paper presents a map of sediment surface distribution and bedforms in the Harle tidal inlet, German Wadden Sea. Data collection, processing, and map editing were realized within the sublittoral mapping program of Lower Saxony national waters carried out by the NLWKN – Coastal Research Station. The map is the result of the combined use of multibeam echosounder, sub-bottom profiler, and ground-truth data. The sediment characterization is achieved by an unsupervised approach using an Object-Based Image Analysis (OBIA) on a normalized backscatter mosaic, verified by nineteen sediment samples. Morphometrical parameters and sub-bottom data provided important information to identify hard substrates and bedforms.

ARTICLE HISTORY

Received 14 April 2022
Revised 23 November 2022
Accepted 27 November 2022

KEYWORDS

Seabed mapping; sediments; bedforms; tidal inlet; Wadden Sea

1. Introduction

The Wadden Sea is among the largest tidal systems in the world encompassing a multitude of transitional zones between land, estuarine, and marine environments. Since 2009 it belongs to the UNESCO World Heritage Site (UNESCO, 2021) and is protected in the framework of the Trilateral Wadden Sea Plan entailing policies, projects, and actions agreed upon by Denmark, Germany, and The Netherlands (Klopper et al., 2022).

The high natural heritage and the substantial presence of economic activities strongly attract the scientific interest in the subtidal environment. At the same time, the mapping and monitoring requirements imposed by European directives force EU-Countries to start research projects on monitoring methods (Winter et al., 2016) as well as extended mapping programs (Klopper et al., 2022).

A long-term monitoring project on the subtidal habitats of the Lower Saxony Wadden Sea is carried out by the NLWKN – Coastal Research Station of Norden, through acquisition and interpretation of different hydro-acoustic datasets and samples (Mascioli & Kunde, 2021). Bathymetry and seabed backscatter are collected simultaneously by means of swath bathymetry systems, in conjunction with sub-bottom profiles and validation samples. These allow the adoption of a robust approach to characterize substrates and bedforms, based on the assumption that there is a close connection among morphology, geomorphological processes, and seabed composition.


The paper presents a map of sediments and bedforms of the subtidal area of the Harle tidal inlet, using methodological approaches largely investigated in the scientific literature (Diesing et al., 2014) and tested in similar test-areas (Mascioli et al., 2017, 2021). Morphometric analyses of bathymetric data provided a quantitative description of seabed morphology. An unsupervised approach based on Object-Based Image Analysis (OBIA) was used to classify and divide acoustic data into different classes, which have been characterized using sediment samples as well as stratigraphic information from sub-bottom profiles and available sediment cores (Bartholomä et al., 2017; Capperucci et al., 2022; NIBIS® Kartenserver, 2020a, 2020b, 2020c).

The map is a product of the mapping program of Lower Saxony Wadden Sea and provides necessary information for the further monitoring of biotopes according to the Habitat Directive 1992/43/EEC, fulfills the requirements of the Marine Strategy Framework Directive 2008/56/EC, and is a necessary input for numerical modeling within morphological evolution studies.

2. Study area

The Wadden Sea stretches off the coasts of the Netherlands, Germany, and Denmark and is separated from the North Sea by the barrier islands of the Frisian archipelago, resulting from Holocene marine

CONTACT Francesco Mascioli  francesco.mascioli@nlwkn.niedersachsen.de  NLWKN, Coastal Research Station, Lower Saxony Water Management, Coastal Defence and Nature Conservation Agency, Jahnstrasse 1, Norden 26506, Germany

 Supplemental map for this article can be accessed at <https://doi.org/10.1080/17445647.2022.2154175>.

© 2022 The Author(s). Published by Informa UK Limited, trading as Taylor & Francis Group on behalf of Journal of Maps

This is an Open Access article distributed under the terms of the Creative Commons Attribution License (<http://creativecommons.org/licenses/by/4.0/>), which permits unrestricted use, distribution, and reproduction in any medium, provided the original work is properly cited.

transgression and concurrent depositional processes (Streif, 2004; Schaumann et al., 2021). The stratigraphic setting consists of a Holocene succession, made of sandy deposits of marine and brackish origin, silt, clay, and intercalated peat layers, lying on a Pleistocene sequence made of sand, silt, and clay of fluvial and glaciofluvial origin. A basal sequence constituted by organic peat sets the limit between Holocene and Pleistocene deposits (Streif, 2004). Tidal currents and wind waves govern the sediment transport and, consequently, erosional and depositional processes acting on seabed and coastline morphology (De Swart & Zimmerman, 2009; Son et al., 2011). Different sized sand waves cover large subtidal sectors. Steep scarps locally bound the slopes of the main tidal channels and outline the presence of peat and cohesive clay layers (Mascioli et al., 2017; Streif, 2004).

The Harle inlet is located between the islands of Spiekeroog, to the West, and Wangerooge, to the East; it features a catchment area of about 65 km² and depth values up to about -34 m NHN (Normalhöhennull, German Standard Elevation Zero) in the northern sector of the main tidal channel. Surficial sediments mainly consist of sands, with a variable mud fraction (Figure 1).

3. Materials and methods

3.1. Dataset

Full coverage high-resolution bathymetry and backscatter were collected by the NLWKN owned survey vessel *Nynorderoog*, by means of a hull-mounted Kongsberg EM2040C multibeam echosounder, operating at 300 kHz and fully compensated for vessel motion (Figure 2). To account for hydrologic effects sound velocity profiles were acquired every 2 h. The Real-Time Kinematic (RTK) positioning technique and the SATellite POsitioning Service (SAPOS®) provided position and elevation. The QPS QINSy software (ver. 8.10) was used to process raw data by accounting for sound velocity, tides, and basic quality control.

Nineteen sediment samples were gathered by the NLWKN owned research vessel *Burchana* (Figure 2), equipped with a 50 L Van Veen grab (Boxes 1 and 2 of the attached map). Number and position of samples were planned based on a preliminary analysis of bathymetric and backscatter data to ground-truth different morphological and acoustical facies (Mascioli et al., 2021). A Kongsberg μ PAP 200 Ultra-Short BaseLine (USBL) underwater positioning system provided the samples position with an accuracy of about 50 cm. This ensured a highly reliable correlation between samples and backscatter by accounting for potential vessel drift due to strong tidal currents.

Sub-bottom profiles were acquired by means of a pole-mounted Kongsberg TOPAS PS120 parametric sub-bottom profiler (Figure 2) using a non-linear wideband Ricker wavelet operating at 6–8 kHz (Box 7 of the attached map). The system provides high-resolution vertical profiles with a maximal penetration of about 5 m. Data were processed using the Delph Seismic Interpretation software (iXblue) for applying tide corrections, enhancing the signal-to-noise ratio, and producing geo-referenced sections.

3.2. Performed analyses

Bathymetrical acoustic data were gridded to a 1 × 1 m cell size Digital Elevation Model (DEM, Box 1 of the attached map). Backscatter was processed by means of QPS FMGeocoder software (ver. 7.9.5) and corrected for system-dependent variables, transmission losses in the water column, insonified area extent on the seafloor and angular response (Beaudoin et al., 2002; Fonseca & Calder, 2005). This allowed the creation of a high-quality artefacts-reduced mosaic of normalized backscatter, that was exported as image with a cell size of 1 × 1 m and used for image-analysis techniques.

Slope, slope standard deviation (STD), profile curvature, and benthic position index (BPI) were derived from the DEM using ArcMap™ 10.6 tools.

Slope is expressed as an angle to the horizontal and indicates the maximum rate of change in elevation value (Box 3 of the attached map). For each cell, it was computed using the average maximum technique given a plane fitting to its 3 by 3 cells neighborhood. Slope values were classified into five classes: flat areas (0°–2°), gently sloping a. (2°–5°), sloping a. (5°–10°), steep a. (10°–20°), and very steep a. (>20°) (Mascioli et al., 2017).

Slope STD was computed within non-overlapping 3 by 3 cells blocks and resulting values were assigned to all of the cells in the block (Box 4 of the attached map). It provided a measure of how far slope values vary from their mean within each block thus providing an index of the surface ruggedness.

Profile curvature was calculated by computing the second derivative of the depth along the direction of maximum slope to outline the presence of convex/concave breaks of slope (Box 5 of the attached map). Profile curvature was expressed in °/m and classified into five classes: very convex areas (< -10°/m), convex a. (-10°–-4°/m), slightly convex a. (-4°–0°/m), slightly concave a. (0°–7°/m), and concave a. (>7°/m) (Mascioli et al., 2017).

Broad- and fine-scale BPI was derived to determine, respectively, long- and short-wavelength features in the landscape. The BPI consists on a focal statistical analysis which evaluates the depth difference between

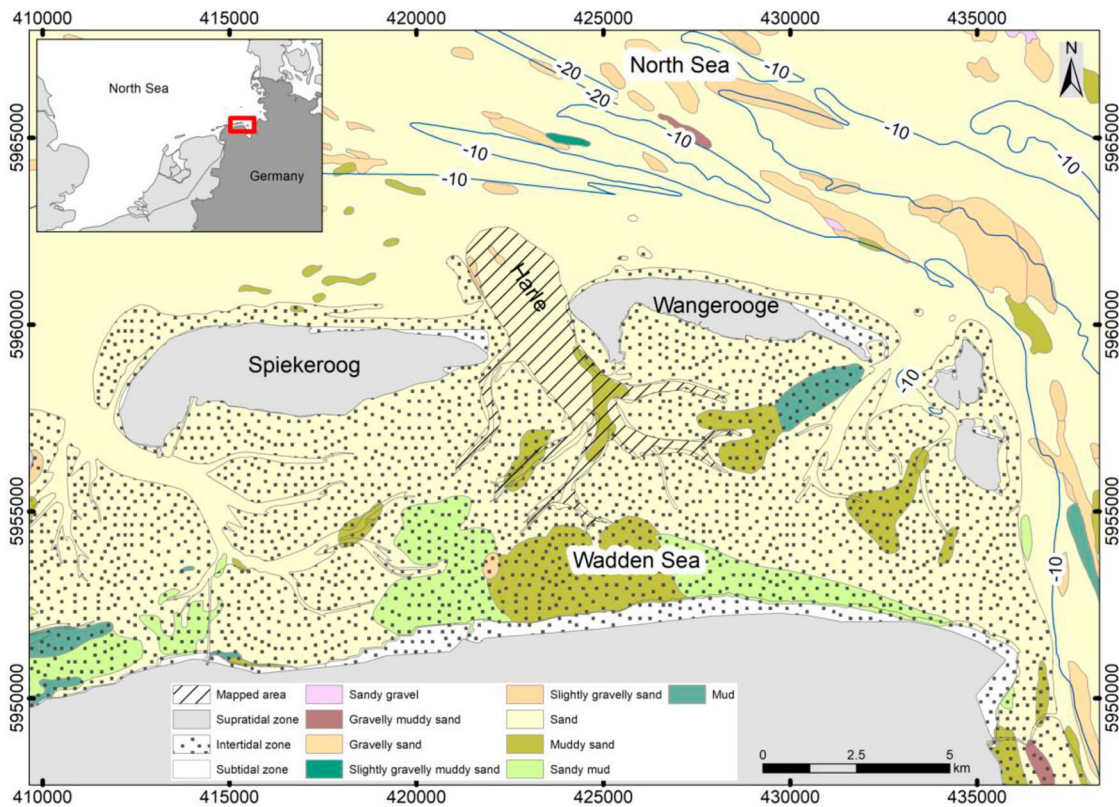


Figure 1. Study area (red polygon) and sediment distribution according to Folk (1954) classification (data from GPDN, 2013).

a cell and the mean depth of surrounding cells, within a user-defined neighborhood geometry (Evans et al., 2016; Lanier et al., 2007; Weiss, 2001). The calculation was executed by means of the Benthic Terrain Modeler 3.0 tool (Walbridge et al., 2018), using an annulus neighborhood shape with inner- and outer-radius values of 20 and 200 m for the broad-scale BPI, 5 and 20 m for the fine-scale BPI. The slope position classification was then performed according to the criteria proposed by Mascioli et al. (2017) (Box 6 of the attached map).

Sediment samples were preliminary analyzed on board through a qualitative description of sample surface, color, particle size, and biogenic content. A subsample was collected to perform laboratory sieve analyses. Particle-size distribution and sample statistics were derived using the Gradistat v.8 software (Blott & Pye, 2001). Samples were classified according to the Folk (1954) classification simplified to four classes (Figure 3) as proposed for harmonizing seabed substrate data of the European Maritime Areas (Kaskela et al., 2019) and used by the seabed-mapping guidelines for the German Bight of German Federal Maritime and Hydrographic Agency (BSH, 2016). The biogenic part, mainly made of shells, was included in the analysis and classified as gravel fraction, if coarser than 2 mm. According to the same guidelines (BSH, 2016), the sand fraction of all samples was further classified based on Figge (1981), in order to characterize the type of sand as a combination of coarse, medium and fine sand (Figure 3).

3.3. Sediments and bedforms mapping

An unsupervised classification was firstly performed on the backscatter image by means of ESRI ArcMap™ 10.6 tools using an OBIA approach (Diesing et al., 2020; Mascioli et al., 2021). The backscatter mosaic was prior segmented using the Segment Mean Shift tool, grouping into segments adjacent pixels that have similar spectral characteristics, thus producing homogenous sectors. Segmented raster was then classified into a number of clusters ranging from 2 up to 15 by means of the ISO-Cluster Unsupervised Classification tool. The optimal number of clusters was not determinable a priori, since it was unknown how many substrate types were actually present and how many of them could be efficiently identified by acoustic data. Its assessment was based on the analysis of the Within and Between Clusters Sum of Squares (WCSS and BCSS). A decrease of the WCSS and an increase of the BCSS is expected as the number of clusters increases, pointing out a progressively higher homogeneity within clusters and a higher differentiation among them. The optimal number of clusters was then derived using the elbow method (Carabella et al., 2022; Mascioli et al., 2021; Tripathi et al., 2018), i.e. by plotting WCSS/BCSS ratios against the number of clusters and by detecting the bend in the plot which states the transition between the best differentiated set of groups and the first exceedingly differentiated one. Detected clusters were given a proper lithological characterization based on the frequency of occurrence of sediments types per cluster.

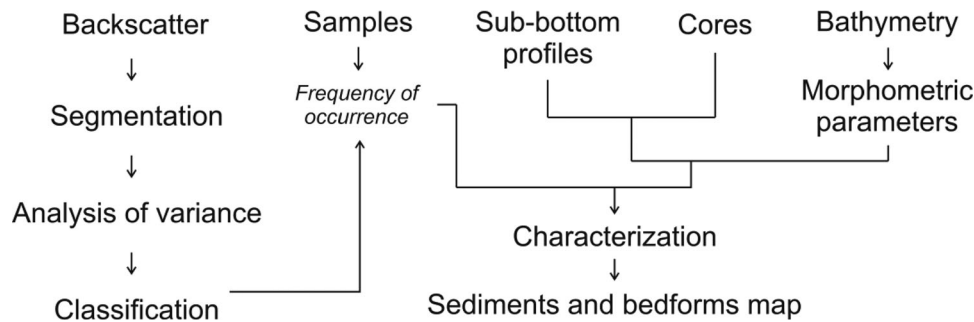


Figure 2. Workflow of the applied mapping methodology.

Sub-bottom data were filtered and tide-corrected. The Relief of the Holocene Basis map provided by the LBEG Geodatabase (NIBIS® Kartenserver, 2020a, 2020b, 2020c), as well as literature data (Schwarzer et al., 2008; Streif, 2004), were used to interpret sub-bottom reflectors. Data were mainly used to infer the presence of peat or cohesive clay, which typically outcrop in correspondence of narrow sectors along steep scarps and therefore are difficult to sample. Consequently, their presence was inferred based on sub-bottom and cores data.

Bedforms mapping was performed based on morphometric parameters derived from bathymetric data and sand waves were classified based on their size and according to Ashley (1990).

4. Results

4.1. Morphometric parameters and geomorphology

Slope values range from 0° up to 60° , with a mean value of 3.5° and standard deviation of 3.5° thus depicting a mostly flat morphology. Wide flats represent over 40% of the area and mainly occur in the shallowest sectors, at the margin of intertidal areas, and in the central part of the Dove Harle tidal channel.

Flats are morphologically quite smooth, as outlined by the general low slope STD, and only locally modeled by small sand waves (Box 7 of the attached map).

Depressions cross flat areas and consist on tidal channels with a flat or u-shaped bottom. At a fine scale, even if extended portions are covered by sand waves, they are characterized by several flat surfaces as well as irregular bedforms. In the northern part, the profile curvature outlines sharp breaks of slope at depths ranging approximately from -5 to -15 m NHN. They bound the very steep slopes which border the deep depression at the end of the H-Groyne and are described by high slope STD values (Box 7 of the attached map).

Slopes mainly consist on the flanks of tidal channels connecting flats and depressions. They are generally gently sloping to sloping surfaces and are extensively covered by sand waves fields (Box 7 of the attached map).

Ridges, at a broad scale, constitute convex surfaces and identify the upper part of slopes, connecting slopes to flats. At a fine scale, they are characterized by very convex surfaces and identify the crests and flanks of sand waves, which feature different shapes and dimensions, going from small to large, and are definitively well described by a general high slope STD (Box 7 of the attached map).

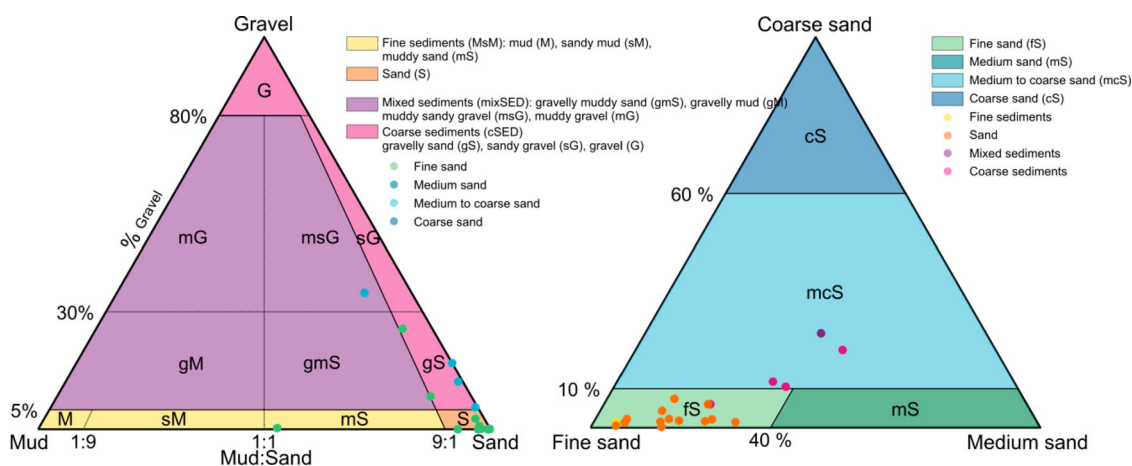


Figure 3. Ground-truths classification according to Folk (1954) as proposed by BSH (2016) (left) and Figue (1981) (right) classifications. Colors of points refer to the legends of classifications.

4.2. Sediment grain-size

Collected samples are made of sandy sediments, with variable fractions of silt, shells and shell fragments (Figure 3).

According to the simplified Folk classification, samples are classified as fine sediments (MsM, 5% of samples), sand (S, 63% of samples), coarse sediments (cSED, 27% of samples), and mixed sediments (mixSED, 5% of samples). According to the Figge classification, the sandy part of collected samples consists of fine sand (fS, 79% of samples) and medium to coarse sand (mcS, 21% of samples).

Fine sediments are represented by one sample, with a mud fraction of about 47% and a fine sand fraction of about 53%; the gravel fraction is lower than 0.5%.

Sands are mainly made of fine sand (fS). The gravel fraction is smaller than 1%, with the exception of just one sample which features a gravel fraction of about 2.5%; the mud fraction is always smaller than 7%.

All coarse sediments are classified as gravelly sand (gS) with a gravel fraction smaller than 30%. The sand fraction is made of medium to coarse sand (mcS, 3 samples) and fine sand (fS, 1 sample).

Mixed sediments are represented by a muddy sandy gravel (msG) sample, with 57% of medium to coarse sand, 36% of gravel, and 7% of mud.

4.3. Segmentation and classification of hydroacoustic data

The analysis of variance performed on segmented acoustic data shows that the WCSS/BCSS ratio quickly decreases increasing from 2 to 4 the number of clusters, and becomes approximately constant for more than 5 groups. Accordingly, the gradient of the curve approaches 0 by increasing the clusters number (Figure 4). Consequently, segments can be fairly grouped into four clusters. A higher number does not improve the differentiation among clusters and does not provide further details to the classification process.

The comparison between samples and classified acoustic data shows that cluster 1 can be characterized as mud and sandy mud with a fine sand fraction, cluster 2 as sand and muddy sand with a fine sand fraction, cluster 3 as coarse sediments with a fine to medium to coarse sand fraction (Table 1). Cluster 4 contains no samples. It consists on very narrow, steep, elongated outcrops located at the border of the deep depression at the end of the H-Groyne. Sub-bottom profiles crossing the depression show a sub-horizontal reflector, which marks a sharp break of slope at about -15 m NHN. Overlying deposits are structured and modeled by bedforms on the surface. Underlying deposits are mostly blind to the sub-bottom profiler. The reflector is almost continuous and can be observed all over the area.

5. Discussion and conclusion

The subtidal area of the Harle inlet is mainly characterized by fine sandy sediments, locally associated to a coarse fraction made of shells and shell fragments. Mud and muddy sands are present as well and located in the shallowest areas, at the margin of intertidal sectors.

The interpretation of the cluster 4 required a combination of different data. The morphology, actually well described by slope, slope STD, profile curvature, and BPI, features very-steep slopes, bounded by sharp convex breaks of slope, strongly different from the rest of the investigated area. This suggests the presence of a hard substrate, outcropping from the sandy sediment. Taking into consideration the sub-bottom profile results and the depth of the Holocene base in the area (NIBIS® Kartenserver, 2020a, 2020b, 2020c), the reflector can be referred to one of the Holocene peat layers (Schaumann et al., 2021; Streif, 2004; see the cross sections in Box 7 of the attached map). A more precise stratigraphic attribution is not possible due to the low resolution of the interpolated Holocene base surface and the absence of cores in this specific area.

Concerning the performed sediment characterization, achieved results show a good consistency with previous maps (GPDN, 2013, 2014). Outcomes from the acoustic classification as presented in this contribution, either way, feature a much higher resolution once more highlighting the reliability of applied methodology. In this context, peat or cohesive clay outcrops mapping by joining cores and hydroacoustic sub-bottom data represents a mandatory step toward a comprehensive seabed characterization.

Detected bedforms feature mainly depositional processes. This is consistent with the historical intense filling trend of the Harle inlet, actually differing from most of the other ones (Homeier et al., 2010).

The main erosive form is the deep depression at the end of the H-Groyne, which makes the Harle inlet one of the deepest of the East Frisian tidal basins and results from the interaction of anthropogenic elements and tidal currents. The groyne, built between 1938 and 1940 to prevent further migration of the inlet toward East, reduces indeed the inlet width, increasing the intensity of tidal currents and enhancing erosive processes (Ladage et al., 2006).

In conclusion, the map provides a detailed representation of sediments and bedforms distribution of a very shallow meso-tidal inlet. The combined use of hydroacoustic and sedimentological data constitutes a highly effective approach, taking a large advantage from the simultaneous collection of backscatter and bathymetry by means of a multibeam echosounder. The critical use of semi-automated approaches

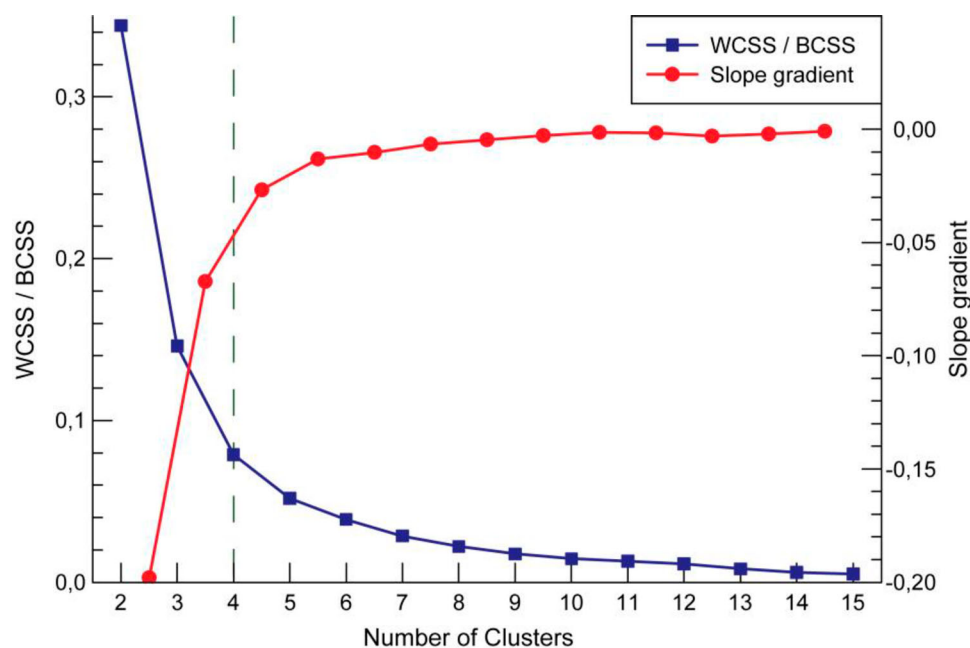


Figure 4. Plot of the within and between clusters sum of squares (WCSS/BCSS) ratio (blue dots and line) and slope gradient of segments joining sequential values (red dots and line). The dashed line indicates the optimum number of clusters.

Table 1. Frequency of occurrence of sediment types per cluster.

OBIA-clusters	Ground-truths					Total
	MsM, fs	S, fs	cSED, fs-mcS	mixSED, mcS	HS	
1	1	0	0	0	0	1
2	0	11	0	0	0	11
3	0	1	5	1	0	7
4	0	0	0	0	0	0
Total	1	12	5	1	0	19

Note: Abbreviations refer to sample classes shown in Figure 3.

ensures the repeatability and objectivity of the mapping process, which are necessary in the frame of monitoring programs. Uncertainties remain still present and are mainly connected to the characterization of hard substrates, due to the small extension of the outcrops which makes the sampling quite difficult. In this case, sub-bottom profiles provide very useful information, although they need to be verified and calibrated by cores.

Software

The QPS QINSy software v.8.10 and the QPS FMGeocoder software v.7.9.5 were used to process raw bathymetry and backscatter data; the iXblue Delph Seismic Interpretation software was used to process sub-bottom data; the Gradistat software v.8 was used to derive particle-size distribution and sample statistics. The Benthic Terrain Modeler 3.0 tool (Walbridge et al., 2018) was used to compute and classify the Benthic Position Index. The vector and raster data and the main map were managed using the ESRI ArcMapTM software v.10.6; final editing of the attached map was performed using Corel Draw 2019[®].

Acknowledgements

This work was realized within the scope of the sublittoral mapping program of Lower Saxony Coastal and Marine Waters, supported by Lower Saxony State in frame of the MSFD. Conceptualization, F.M.; data collection and processing, F.M., T.K.; interpretation, F.M., F.C., V.P.; original draft preparation, review and editing, F.M., V.P., J.C.; map editing, F.M., V.P., J.C.; supervision, F.M., E.M. All authors provided critical feedback and helped to shape the manuscript. All authors have read and agreed to the published version of the manuscript.

Disclosure statement

No potential conflict of interest was reported by the author(s).

Funding

This research did not receive any specific grant from funding agencies in the public, commercial, or not-for-profit sectors.

Data availability statement

The data that support the findings of this study are available from the corresponding author, upon reasonable request. Raw and derived data were generated by the NLWKN, Lower Saxony Water Management, Coastal Defence and Nature Conservation Agency.

ORCID

Francesco Mascioli  <http://orcid.org/0000-0001-9968-5297>
 Valerio Piattelli  <http://orcid.org/0000-0001-9101-5897>
 Francesco Cerrone  <http://orcid.org/0000-0003-1861-0133>
 Jacopo Cinosi  <http://orcid.org/0000-0002-2628-3382>
 Tina Kunde  <http://orcid.org/0000-0002-8611-9891>
 Enrico Miccadei  <http://orcid.org/0000-0003-2114-2940>

References

- Ashley, G. M. (1990). Classification of large-scale subaqueous bedforms; a new look at an old problem. *Journal of Sedimentary Research*, 60(1), 160–172. <https://doi.org/10.2110/jsr.60.160>
- Bartholomä, A., Bittmann, F., Blume, K., Bungenstock, F., Capperucci, R., Enters, D., Haynert, K., Hüser, A., Kunde, T., Mascioli, F., Peis, K., Scheder, J., Schlüt, F., Siegmüller, A., Wehrmann, A., Wurpts, A., & Zolitschka, B. (2017, May, 8–11). WASA—The Wadden Sea as an archive of landscape evolution, climate change and settlement history – perspectives and preliminary results. The 14th international scientific Wadden Sea Symposium (ISWSS 14), Abstract Volume, 22–23, TØnder, Dänemark.
- Beaudoin, J., Hughes Clarke, J. E., Van den Aemele, E. J., & Gardner, J. V. (2002, May, 28–31). *Geometric and radiometric correction of multibeam backscatter derived from Reson 8101 systems*. Proceedings of the Canadian Hydrographic Conference, Toronto, Canada.
- Blott, S. J., & Pye, K. (2001). Gradistat: A grain size distribution and statistics package for the analysis of unconsolidated sediments. *Earth Surface Processes and Landforms*, 26, 1237–1248. <https://doi.org/10.1002/esp.261>
- BSH. (2016). *Anleitung zur Kartierung des Meeresbodens Mittels Hochauflösender Sonare in den Deutschen Meeresgebieten* (1 Vol. BSH-Nr. 7201). Hamburg and Rostock: Bundesamt für Seeschifffahrt und Hydrographie (BSH).
- Capperucci, R., Bartholomä, A., Bungenstock, F., Enters, D., Karle, M., & Wehrmann, A. (2022). The WASA core catalogue of Late Quaternary depositional sequences in the central Wadden Sea – a manual for the core repository. *Netherlands Journal of Geosciences*, 101, e5. <https://doi.org/10.1017/njg.2022.1>
- Carabella, C., Cinosi, J., Piattelli, V., Burrato, P., & Miccadei, E. (2022). Earthquake-induced landslides susceptibility evaluation: A case study from the Abruzzo region (Central Italy). *Catena*, 208. <https://doi.org/10.1016/j.catena.2021.105729>
- De Swart, H., & Zimmerman, J. T. F. (2009). Morphodynamics of tidal inlet systems. *Annual Review of Fluid Mechanics*, 41(1), 203–229. <https://doi.org/10.1146/annurev.fluid.010908.165159>
- Diesing, M., Green, S. L., Stephens, D., Lark, R. M., Stewart, H. A., & Dove, D. (2014). Mapping seabed sediments: Comparison of manual, geostatistical, object-based image analysis and machine learning approaches. *Continental Shelf Research*, 34, 107–119. <https://doi.org/10.1016/j.csr.2014.05.004>
- Diesing, M., Mitchell, P., O’Keeffe, E., Montereale-Gavazzi, G., & Le Bas, T. (2020). Limitations of predicting substrate classes on a sedimentary complex but morphologically simple seabed. *Remote Sensing*, 12(20), 3398. <https://doi.org/10.3390/rs12203398>
- Evans, D. A., Williard, K. W., & Schoonover, J. E. (2016). Comparison of terrain indices and landform classification procedures in low-relief agricultural fields. *Journal of Geospatial Applications in Natural Resources*, 1(1), 1–17. https://scholarworks.sfasu.edu/j_of_geospatial_applications_in_natural_resources/vol1/iss1/1
- Figge, K. (1981). Karte und Begleitheft zur Karte der Sedimentverteilung in der Deutschen Bucht, Maßstab 1:250.000. Deutsches Hydrographisches Institut, Hamburg.
- Folk, R. L. (1954). The distinction between grain size and mineral composition in sedimentary-rock nomenclature. *The Journal of Geology*, 62(4), 344–359. <https://doi.org/10.1086/626171>
- Fonseca, L., & Calder, B. (2005, March 29–31). *Geocoder: an efficient backscatter map constructor*. Proceedings of the U.S. Hydrographic Conference, 9 pp, Hydrographic Society of America, San Diego, CA, USA.
- GPDN. (2013). Erstellung der Karte zur Sedimentverteilung auf dem Meeresboden in der deutschen Nordsee nach der Klassifikation von Folk (1954, 1974) – Nordsee Kartenserver. www.gpdn.de
- GPDN. (2014). Erstellung der Karte zur Sedimentverteilung auf dem Meeresboden in der deutschen Nordsee nach der Klassifikation von Figge (1981) – Nordsee Kartenserver. www.gpdn.de
- Homeier, H., Stephan, H.-J., & Niemeyer, H. D. (2010). Historische Kartenwerk Niedersächsische Küste der Forschungsstelle Küste. *Berichte der Forschungsstelle Küste*, 43, 133.
- Kaskela, A. M., Kotilainen, A. T., Alanen, U., Cooper, R., Green, S., Guinan, J., van Heteren, S., Kihlman, S., Van Lancker, V., Stevenson, A., & the EMODnet Geology Partners (2019). Picking p the pieces – harmonising and collating seabed substrate data for European maritime areas. *Geosciences*, 9(2), 84. <https://doi.org/10.3390/geosciences9020084>
- Klopper, S., Bostelmann, A., Bregnballe, T., Busch, J. A., Buschbaum, C., Deen, K., Dönnick, A., Gutow, L., Jensen, K., Jepsen, N., Luna, S., Meise, K., Teilmann, J., & van Wezel, A. (2022). Wadden Sea Quality Status Report. Common Wadden Sea Secretariat, Wilhelmshaven, Germany. Downloaded 07.09.2022. qsr.waddensea-worldheritage.org/reports/subtidal-habitats.
- Ladage, F., Stephan, H. J., & Niemeyer, H. D. (2006). Interactions of large-scale Groyne and tidal inlet migration. In *Coastal dynamics 2005: State of the practice* (pp. 1–14). [https://doi.org/10.1061/40855\(214\)111](https://doi.org/10.1061/40855(214)111)
- Lanier, A., Romsos, C., & Goldfinger, C. (2007). Seafloor habitat mapping on the Oregon continental margin: A spatially nested GIS approach to mapping scale, mapping methods, and accuracy quantification. *Marine Geodesy*, 30(1–2), 51–76. <https://doi.org/10.1080/01490410701296143>
- Mascioli, F., Bremm, G., Bruckert, P., Tants, R., Dirks, H., & Wurpts, A. (2017). The contribution of geomorphometry to the seabed characterization of tidal inlets (Wadden Sea, Germany). *Zeitschrift für Geomorphologie, Supplementary Issues*, 61(2), 179–197. https://doi.org/10.1127/zfg_suppl/2017/0354
- Mascioli, F., & Kunde, T. (2021). Sedimentkartierung in der niedersächsischen Nordsee und im Wattenmeer. *Hydrographische Nachrichten, Journal of Applied Hydrography*, 120, 24–31. <https://doi.org/10.23784/HN120-03>
- Mascioli, F., Piattelli, V., Cerrone, F., Gasprino, D., Kunde, T., & Miccadei, E. (2021). Feasibility of objective seabed mapping techniques in a coastal tidal environment (Wadden Sea, Germany). *Geosciences*, 11(2), 49. <https://doi.org/10.3390/geosciences11020049>
- NIBIS® Kartenserver. (2020a). *Boreholes and profiles*. Landesamt für Bergbau, Energie und Geologie (LBEG). <https://nibis.lbeg.de/cardomap3/>
- NIBIS® Kartenserver. (2020b). *Profiletypes of the coastal Holocene*. Landesamt für Bergbau, Energie und Geologie (LBEG). <https://nibis.lbeg.de/cardomap3/>

- NIBIS® Kartenserver. (2020c). *Relief of the Holocene basis*. Landesamt für Bergbau, Energie und Geologie (LBEG). <https://nibis.lbeg.de/cardomap3/>
- Schaumann, R. M., Capperucci, R. M., Bungenstock, F., McCann, T., Enters, D., Wehrmann, A., & Bartholomä, A. (2021). The middle Pleistocene to early Holocene sub-surface geology of the Norderney tidal basin: New insights from core data and high-resolution sub-bottom profiling (Central Wadden Sea, Southern North Sea). *Netherlands Journal of Geosciences*, 100, e15. <https://doi.org/10.1017/njg.2021.3>
- Schwarzer, K., Ricklefs, K., Bartholomä, A., & Zeiler, M. (2008). Geological development of the North Sea and the Baltic Sea. *Die Küste*, 74, 1–17. <https://hdl.handle.net/20.500.11970/101590>
- Son, C. S., Flemming, B. W., & Bartholomä, A. (2011). Evidence for sediment recirculation on an ebb-tidal delta of the East Frisian barrier island system, southern North Sea. *Geo-Marine Letters*, 31(2), 87–100. <https://doi.org/10.1007/s00367-010-0217-8>
- Streif, H. (2004). Sedimentary record of Pleistocene and Holocene marine inundations along the North Sea coast of Lower Saxony, Germany. *Quaternary International*, 112(1), 3–28. [https://doi.org/10.1016/S1040-6182\(03\)00062-4](https://doi.org/10.1016/S1040-6182(03)00062-4)
- Tripathi, S., Bhardwaj, A., & Eswaran, P. (2018). Approaches to clustering in customer segmentation. *International Journal of Engineering & Technology*, 7(3.12), 802. <https://doi.org/10.14419/ijet.v7i3.12.16505>
- UNESCO. (2021). *World heritage list*. Retrieved April 12, 2021, from <https://whc.unesco.org/en/list/1314>
- Walbridge, S., Slocum, N., Pobuda, M., & Wright, D. J. (2018). Unified geomorphological analysis workflows with benthic terrain modeler. *Geosciences*, 8(3), 94. <https://doi.org/10.3390/geosciences8030094>
- Weiss, A. (2001, July 9–13). *Topographic Position and Landforms Analysis*. ESRI User Conference, San Diego, CA, USA.
- Winter, C., Backer, V., Adolph, W., Bartholomä, A., Becker, M., Behr, D., Callies, U., Capperucci, R., Ehlers, M., Farke, H., Geimecke, C., Grayek, S., Hass, C., Heipke, C., Herrling, G., Hillebrand, H., Hodapp, D., Holler, P., Jung, R., ... Wirtz, K. (2016). *Wissenschaftliche Monitoringkonzepte für die Deutsche Bucht (WIMO) – Abschlussbericht*, [Miscellaneous]. <http://doi.org/10.2314/GBV:860303926>